JACS
JOURNAL OF THE AMERICAN CHEMICAL SOCIETY
pubs.acs.org/JACS
Article

Molecular Basis of Small-Molecule Binding to α-Synuclein

Paul Robustelli, Alain Ibanez-de-Opakua, Cecily Campbell-Bezat, Fabrizio Giordanetto, Stefan Becker, Markus Zweckstetter,* Albert C. Pan,* and David E. Shaw*

Cite This: J. Am. Chem. Soc. 2022, 144, 2501−2510
Read Online
ACCESS | Metrics & More | Article Recommendations | Supporting Information

ABSTRACT: Intrinsically disordered proteins (IDPs) are implicated in many human diseases. They have generally not been amenable to conventional structure-based drug design, however, because their intrinsic conformational variability has precluded an atomic-level understanding of their binding to small molecules. Here we present long-time-scale, atomic-level molecular dynamics (MD) simulations of monomeric α-synuclein (an IDP whose aggregation is associated with Parkinson's disease) binding the small-molecule drug fasudil in which the observed protein−ligand interactions were found to be in good agreement with previously reported NMR chemical shift data. In our simulations, fasudil, when bound, favored certain charge−charge and π-stacking interactions near the C terminus of α-synuclein but tended not to form these interactions simultaneously, rather breaking one of these interactions and forming another nearby (a mechanism we term *dynamic shuttling*). Further simulations with small molecules chosen to modify these interactions yielded binding affinities and key structural features of binding consistent with subsequent NMR experiments, suggesting the potential for MD-based strategies to facilitate the rational design of small molecules that bind with disordered proteins.

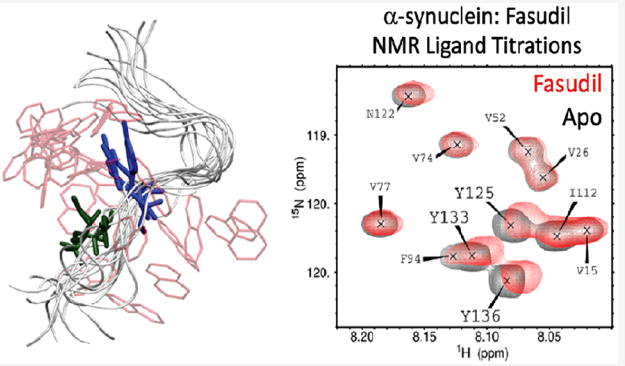

INTRODUCTION

Intrinsically disordered proteins (IDPs), which lack a fixed three-dimensional structure under native, functional conditions, play important roles in a large number of biological pathways.[1−6] IDPs and proteins with large disordered regions represent approximately 40% of the protein-coding human genome[1,7] and are also crucial components of biomolecular condensates, which have been increasingly recognized to be important regulators of cellular processes.[8] IDPs are implicated in many human diseases, such as cancer, cardiovascular disease, diabetes, and neurodegeneration, and represent a large pool of potential drug targets.[9−15] Drugging IDPs, however, has proven difficult due to their highly conformationally dynamic nature and the challenges associated with experimentally characterizing their conformational ensembles at atomic resolution.[16−22] Because IDPs generally cannot be meaningfully represented by a single dominant conformation, or even a small number of substantially populated conformations, they are generally not suitable targets for conventional structure-based drug design methods, in which small molecules are designed to optimize interactions with a particular binding pocket in a folded protein.[10−13,23]

The aggregation of the IDP α-synuclein (α-syn) into oligomers and amyloid fibrils may play an important role in the etiology of Parkinson's disease,[21,24] and a potential therapeutic strategy for Parkinson's disease is the stabilization of α-syn in its soluble monomeric form. Recently, the small molecule fasudil has been shown to interact with monomeric α-syn and delay its aggregation. Solution nuclear magnetic resonance (NMR) experiments demonstrated that this interaction is primarily localized to a specific cluster of protein residues at the C terminus.[25] In contrast to a "lock-and-key" picture of protein−ligand recognition, in which a ligand binds to a stable and well-defined binding site, this fairly specific interaction between the ligand and the protein occurs while the protein remains highly dynamic and disordered. A detailed molecular picture of how fasudil binds to α-syn could shed light on how fasudil recognizes a specific region of disordered α-syn monomer, and provide a basis for the rational design of molecules that bind more strongly.

Atomic-level molecular dynamics (MD) simulations have been a valuable tool for complementing experimental measurements of disordered proteins and providing detailed descriptions of their conformational ensembles.[26−31] Recent improvements to molecular mechanics potential energy functions, or "force fields", have dramatically improved the accuracy of MD simulations of disordered proteins, as assessed

Received: July 21, 2021
Published: February 8, 2022

https://doi.org/10.1021/jacs.1c07591
J. Am. Chem. Soc. 2022, 144, 2501−2510

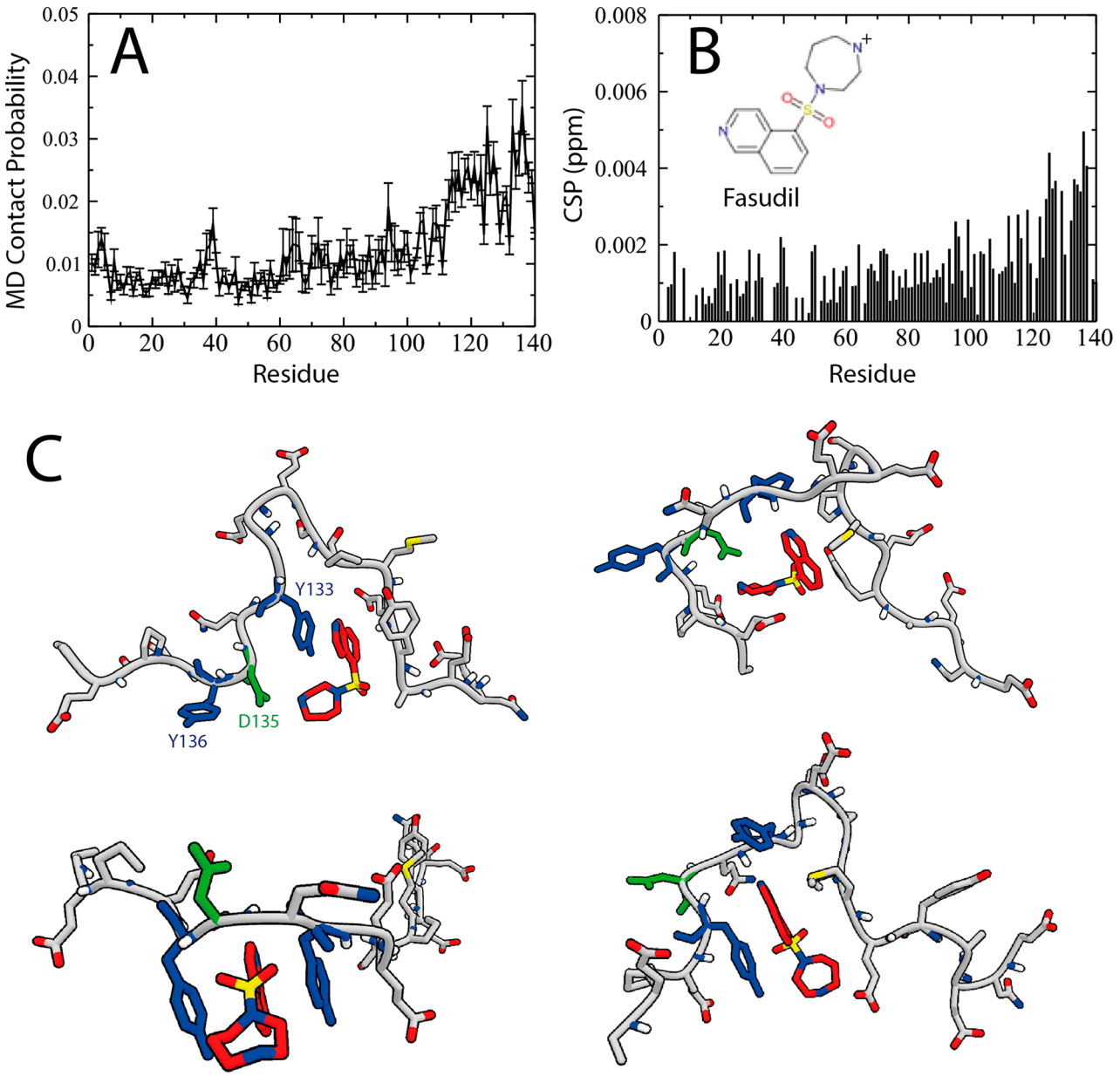

Figure 1. The dynamic binding mechanism of fasudil with α-synuclein observed in MD simulations is consistent with NMR chemical shift perturbation experiments. (A) Contact probabilities between each residue of α-synuclein and fasudil observed in an unbiased 1.5 ms MD simulation run with the a99SB-*disp* force field. A contact is assigned to all MD frames when the minimum distance between any atom of fasudil and any heavy atom of a protein side-chain residue is <6 Å. Error bars were calculated by blocking (see SI for more details). (B) NMR chemical shift perturbations of α-synuclein measured in the presence of 2.7 mM fasudil. Perturbations in the chemical shift values for ^{1}H and ^{15}N were calculated as $[(\Delta\delta^{1}\mathrm{H})^{2} + (\Delta\delta^{15}\mathrm{N}/10)^{2}]^{1/2}$. (C) Snapshots of binding modes of fasudil (red carbons) with α-syn-C-term, illustrating the conformational diversity of the bound ensemble. The residues with the highest probability of interacting with fasudil in the bound ensemble are colored blue (Y133, Y136) and green (D135).

by their agreement with a wide variety of experimental measurements.[32−41] MD simulations with these improved force fields have shown promise for describing molecular recognition mechanisms of IDPs in scenarios such as folding-upon-binding,[42] dimerization,[43] and the formation of higher-order molecular assemblies.[44,45] MD simulations may also provide a promising approach for describing the binding of small molecules to disordered proteins in atomistic detail and for investigating the driving forces of these interactions.[11,23,46−53]

Here we report long-time-scale MD simulations of fasudil binding to α-syn. The probability of observing contacts between fasudil and α-syn correlated remarkably well in our simulations with the magnitude of NMR chemical shift perturbations measured from α-syn−fasudil titrations. This correlation suggests that these simulations provide a highly accurate description of the molecular interactions that give rise to the preferential binding of fasudil to the C-terminal region of α-syn, which we found to be driven mainly by combinations of aromatic stacking and charge−charge interactions. The simulations provide an atomically detailed picture of the protein−ligand binding ensemble—in which α-syn remained largely disordered while fasudil transitioned between several distinct binding modes—and illustrate how a set of weak

https://doi.org/10.1021/jacs.1c07591
J. Am. Chem. Soc. 2022, 144, 2501−2510

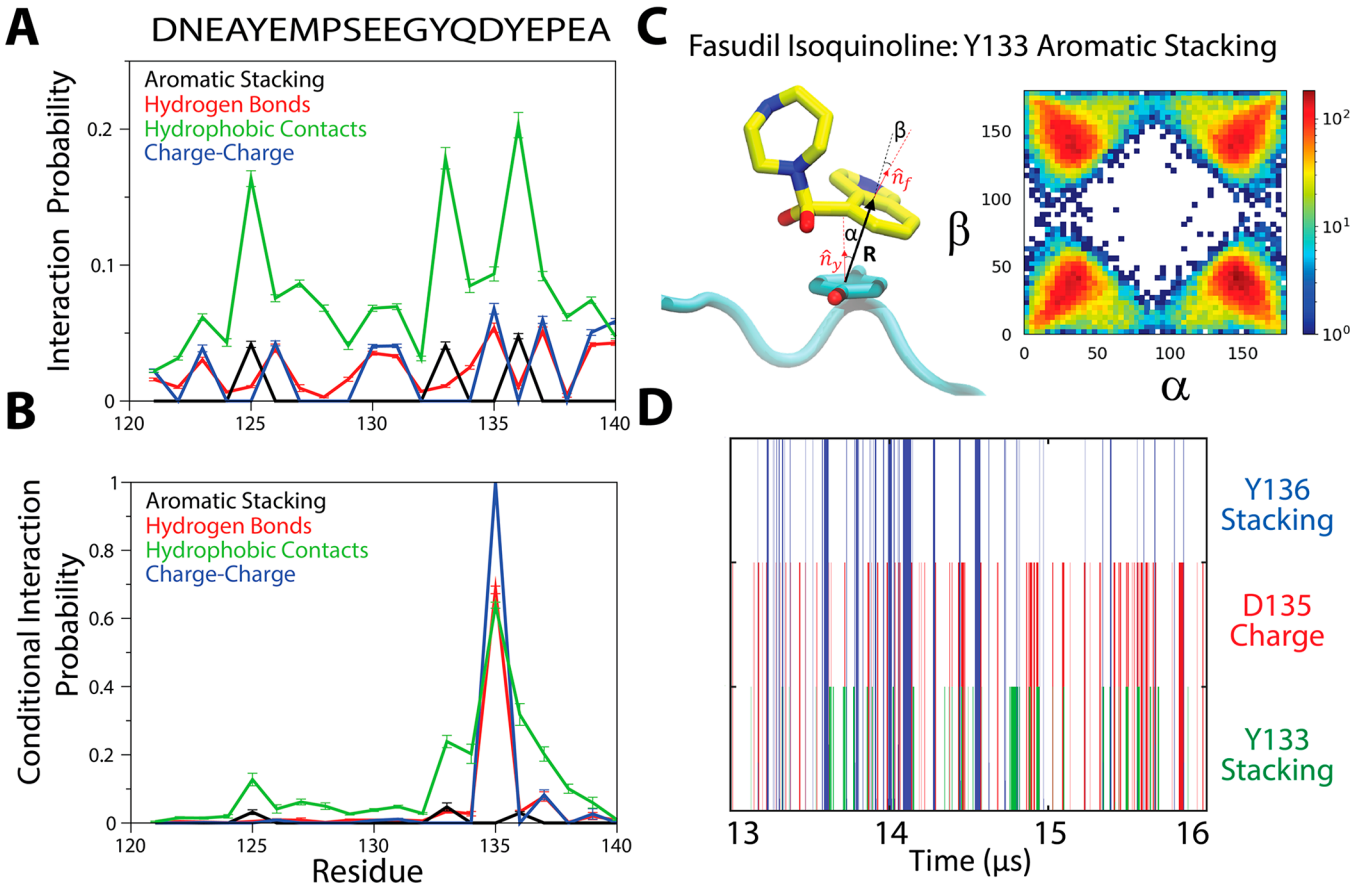

Figure 2. When in contact with α-synuclein, fasudil dynamically shuttled between different binding modes with different interactions; multiple specific interactions were rare in any given binding mode. (A) The probability of observing interactions between fasudil and α-syn-C-term categorized by type of interaction in the bound ensemble. We note that a given residue can only form certain types of interactions. Error bars were calculated by blocking (see SI for more details). (B) Conditional interaction probability of observing a specific interaction between α-synuclein and fasudil in the bound ensemble, given that a charge−charge interaction had formed between D135 and fasudil. (C) Illustration of the stacking orientation between fasudil's isoquinoline ring and the Y133 side chain. **R** is the distance vector between the centers of mass of the six aromatic carbons of Y133 and ten aromatic atoms of the isoquinoline ring on fasudil. The distributions are normalized and shown on a logarithmic scale. (D) Time series of a representative portion of the unbiased MD trajectory of α-synuclein with fasudil showing the formation of different interactions. The presence of a line indicates the formation of a particular interaction. Trajectory frames were sampled every 180 ps.

intermolecular interactions can lead to a small molecule interacting with a specific part of a protein that remains highly dynamic upon binding. We observed that although fasudil had a preference for a set of specific protein−ligand interactions, multiple such interactions rarely formed simultaneously. Instead, binding occurred through what we refer to as a *dynamic shuttling* mechanism, in which one of these preferred interactions broke before another formed nearby.

To better understand small-molecule features that confer affinity and specificity and to prospectively test the accuracy of our MD models, we simulated α-syn with a library of 49 small molecules that were selected to probe the simulated binding interactions and modify protein−ligand affinity. Subsequent NMR measurements of a subset of these small molecules showed that their relative binding affinities were in line with our computational predictions, and also provided support for key structural features of the simulated binding interactions, such as the populations of intermolecular hydrogen bonds and of aromatic stacking interactions. These observations illustrate that MD simulations can be a valuable tool for describing the binding of small molecules to disordered proteins, and suggest potential strategies for the rational design of molecules that bind disordered protein sequences with higher affinity and greater specificity.

RESULTS AND DISCUSSION

We performed a 1.5 ms MD simulation of α-syn and fasudil using the a99SB-*disp* force field[33] and the generalized amber force field (GAFF) for fasudil.[54,55] The probability of observing contacts between fasudil and each residue of α-syn is shown in Figure 1A. We also measured backbone ^{15}N and $^{1}H_N$ NMR chemical shift perturbations (CSPs) of α-syn in the presence and absence of 2.7 mM fasudil. CSPs are sensitive to changes in the local chemical environment of each backbone amide bond, and are thus sensitive probes of protein−ligand interactions. The magnitude of the NMR CSPs is shown in Figure 1B. In agreement with previous measurements,[25] we observed CSPs throughout the entire sequence of α-syn, with the largest-magnitude CSPs observed in the C-terminal residues 121−140.

The probability of observing contacts between fasudil and α-syn in the simulation and the magnitude of NMR CSPs measured for each residue are in excellent agreement (Figure S1, Pearson correlation coefficient, r = 0.67). Consistent with the experimental CSPs, in simulation we observed that fasudil

https://doi.org/10.1021/jacs.1c07591
J. Am. Chem. Soc. 2022, 144, 2501−2510

interacts somewhat weakly with the entire α-syn sequence, but has a higher affinity for residues 121−140. The relatively small magnitude of the CSPs observed suggests that the underlying conformational ensemble of α-syn is not substantially altered in the presence of fasudil, and thus that α-syn remains disordered while interacting with fasudil. In simulation, we also found no large-scale differences between the conformational ensembles of the bound and unbound states of α-syn (Figures S2 and S5)—nor between the conformational ensembles of bound and unbound states of fasudil (Figure S2)—and that the bound ensemble is not dominated by a single conformation or a small number of substantially populated conformations (Figure S3). These results illustrate that the recently developed a99SB-*disp* force field,[33] which provides improved descriptions of disordered proteins, is capable of identifying the binding sites of a small molecule in the context of an entire disordered protein sequence, and suggest that our simulation provides a meaningful model of the interactions between α-syn and fasudil.

In order to obtain a better understanding of the bound protein−ligand ensemble and the intermolecular interactions that confer specificity of fasudil to the C terminus of α-syn, we performed additional simulations of fasudil and a truncated α-syn construct containing only the region of α-syn to which fasudil preferentially binds (residues 121−140), which we will refer to as *α-syn-C-term*. Using this construct enabled more efficient simulation (given the smaller sizes of the protein and water box), which allowed us to obtain better statistics on the populations of dominant intermolecular interactions and the distributions of the α-syn conformations in bound states. Importantly, simulations with the reduced construct produced a similar contact probability with fasudil when compared to full-length α-syn (Figure S4). Simulations of full-length α-syn with fasudil also did not appear to involve long-range protein contacts that influenced small-molecule binding (Figure S5), implying that the simulation of full-length α-syn may not be required to model how fasudil binds to the C-terminal region and further justifying the use of a smaller protein construct. Similarly to simulations of full-length α-syn, simulations of fasudil with α-syn-C-term did not give rise to substantially populated long-range protein contacts (Figure S5) or display a substantial difference between the conformational ensembles of bound and unbound states (Figures S6 and S15).

We found that, although bound protein−ligand conformations (i.e., those in which there was at least one contact between the protein and the ligand) exhibited a heterogeneity of binding modes (Figure 1C) instead of a single, stable protein−ligand complex (or a small number of them), we did observe a preference for specific charge−charge and aromatic π-stacking protein−ligand interactions near the C-terminus (Figure 2). In Figure 2A, we break down the protein−ligand contacts into specific physical interactions and present the probability of observing hydrophobic contacts, charge−charge interactions, aromatic π-stacking interactions, and hydrogen bonds between fasudil and each residue of α-syn-C-term in bound conformations. We found that the relative populations of protein−ligand interactions varied among similar amino acids in the α-syn sequence. That is, aromatic side chains did not all have the same propensity to form hydrophobic contacts and aromatic π-stacking interactions, and not all negatively charged side chains had the same propensity to form charge−charge interactions with fasudil.

Excluding hydrophobic contacts, which are relatively nonspecific, the most likely interactions were a charge−charge contact between the positively charged amine of fasudil's azepane ring and the side chains of D135 and E137, and aromatic π-stacking interactions between fasudil's isoquinoline ring and the side chains of Y133 and Y136. The most populated interactions are localized to regions where negatively charged residues neighbor aromatic residues. The populations of interactions in those regions do not seem to depend solely on having an aromatic residue next to a negatively charged residue, however, as the stacking and charge−charge interactions between fasudil and D135 and Y136, taken together, are more populated than those between fasudil and Y125 and E126 (Figure 2A), suggesting a coupling of intermolecular interactions beyond those between the ligand and these two neighboring residues.

Examination of the bound-state ensemble suggests that increased affinity between fasudil and specific residues in the α-syn-C-term sequence cannot be explained by the simultaneous formation of multiple specific interactions within individual conformations of the bound ensemble. If we consider only conformations where fasudil had a charge−charge interaction with D135, for example (the most likely charge−charge interaction between the protein and the ligand; Figure 2A), very few of those conformations also made an additional specific protein−ligand interaction (Figure 2B). Only two interactions—aromatic stacking interactions with Y133 and charge−charge interactions with E137—were formed in >4% of MD frames in which fasudil also formed charge interactions with D135. These observations about the lack of multiple specific protein−ligand interactions in the bound ensemble are also corroborated by a mutual information analysis: calculating the mutual information between different protein−ligand interactions shows very little coupling between different interactions (Figure S7). Instead, we observed that the formation of a single intermolecular contact often spatially localized and oriented fasudil such that additional intermolecular interactions, although not forming simultaneously, became accessible later in time with relatively small ligand displacements.

To better understand the nature of the coupling among interactions, we sought to determine the extent to which the formation of specific intermolecular interactions could geometrically orient fasudil relative to α-syn, even as α-syn remained highly dynamic. We thus examined the distribution of π-stacking orientations[56] of the isoquinoline ring of fasudil with side chains of Y125, Y133, and Y136 to determine how the identity of neighboring residues influenced the distribution of orientations of these interactions. For all conformations in which the ring centers of the fasudil isoquinoline group and a tyrosine phenol group were within 5 Å, we calculated the orientations of the normal vectors of each ring plane relative to a vector connecting the two ring centers (Figure 2C, left panel). If fasudil were interacting with an isolated tyrosine with no preferred geometric orientation, one would expect the four quadrants of a graph representing the distribution of the orientations of the ring plane normal vectors to be equally populated. That is, the isoquinoline ring would have an equal probability of stacking above or below the tyrosine phenol ring, and would have an equal probability of facing upward or downward in either position. We note that each tyrosine had slightly asymmetric distributions of π-stacking orientations, and that there was not a consistent trend in the populations of

https://doi.org/10.1021/jacs.1c07591
J. Am. Chem. Soc. 2022, 144, 2501−2510

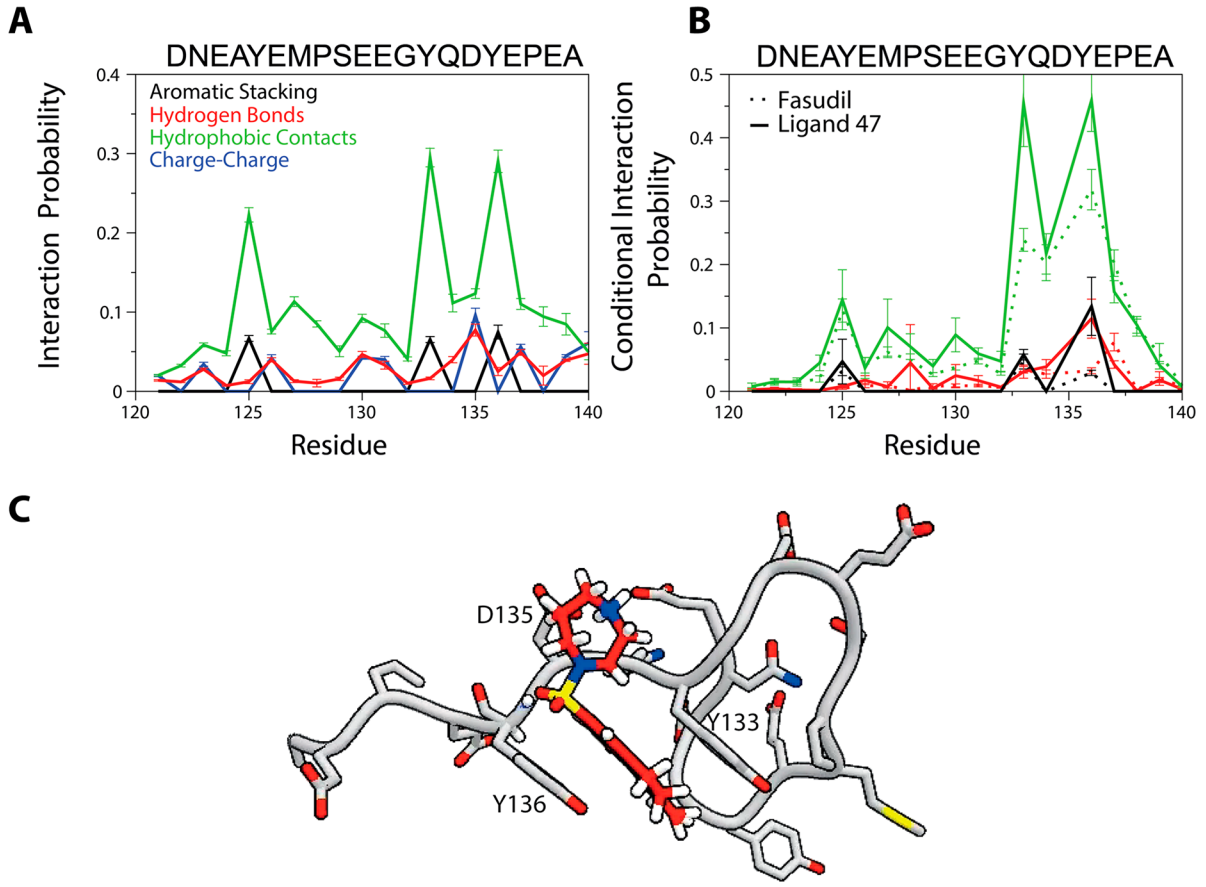

Figure 3. Predicted interactions of ligand 47 with α-synuclein. (A) Interaction probabilities for each residue 121−140 of α-synuclein and ligand 47 observed in an unbiased MD simulation. (B) The conditional probability of observing interactions between α-synuclein and ligand 47, and between α-synuclein and fasudil, for all conformations containing a charge−charge contact with D135. The values at D135 have been omitted for better visualization of the differences between the two ligands. Error bars were calculated by blocking (see SI for more details). (C) Representative structure of the most populated cluster of conformations of the ligand 47 bound ensemble. In this conformation, ligand 47 (red carbons) can simultaneously stack with Y136, form a hydrogen bond with the backbone amide of Y136, and form charge contacts with D135.

each orientation among the tyrosines (Figures 2C and S8; Table S1). This suggests that the conformations of the neighboring residues influence the relative free energies of each possible stacking orientation.

The distribution of π-stacking orientations observed between fasudil and Y133 is shown in Figure 2C (right panel). We observed that the most populated stacking orientation ($\alpha > 90°$, $\beta < 90°$, quadrant 4 in Table S1) was only slightly more populated (116%) than was the least populated orientation ($\alpha > 90°$, $\beta > 90°$, quadrant 2 in Table S1). We found, however, that the asymmetry in the distribution of π-stacking orientations was substantially larger when considering only conformations in which fasudil also formed a charge−charge contact with D135 (Table S1): ~270% enrichment for ($\alpha > 90°$, $\beta < 90°$) relative to ($\alpha < 90°$, $\beta < 90°$) (Table S1). A similar effect—enrichments of 288% for ($\alpha > 90°$, $\beta > 90°$) relative to ($\alpha > 90°$, $\beta < 90°$) and 140% for ($\alpha < 90°$, $\beta > 90°$) relative to ($\alpha > 90°$, $\beta < 90°$)—was observed for Y125 and Y136, respectively, in the presence of D135 charge contacts. This illustrates that the presence of charge−charge contacts confers a set of preferential orientations of fasudil relative to neighboring aromatic residues.

We note that fasudil only rarely simultaneously formed both π-stacking interactions and charge−charge contacts in the bound ensemble. We observed both π-stacking interactions and charge−charge contacts in only 0.27%, 0.38%, and 0.68% of the bound ensemble for residues Y125, Y133, and Y136, respectively. The average population of conformations in which there were both π-stacking interactions and charge−charge contacts was 0.20% of the bound ensemble. It thus appears that the presence of asymmetries in the distribution of π-stacking orientations in the bound ensemble cannot be accounted for solely by the simultaneous formation of charge−charge and π-stacking interactions. This suggests that the proximity and distribution of spatial orientations of the α-syn side chains confer a preferred set of orientations of fasudil relative to α-syn as fasudil dynamically shuttles between complementary intermolecular interactions.

We illustrate this example of the dynamic shuttling of fasudil and α-syn between complementary intermolecular interactions in Figure 2D with a time series of the formation of different intermolecular interactions. Temporal correlations among these interactions persist for as long as 100 ns (Figure S8B). The probability, for example, of observing a π-stacking interaction between fasudil and Y136 after observing a charge−charge interaction between fasudil and D135 is greater than random for almost 100 ns, whereas the average lifetime of configurations with simultaneous interactions between fasudil and D135 and Y136 is only 570 ps. Although multiple interactions rarely formed simultaneously, fasudil transiently

https://doi.org/10.1021/jacs.1c07591
J. Am. Chem. Soc. 2022, 144, 2501−2510

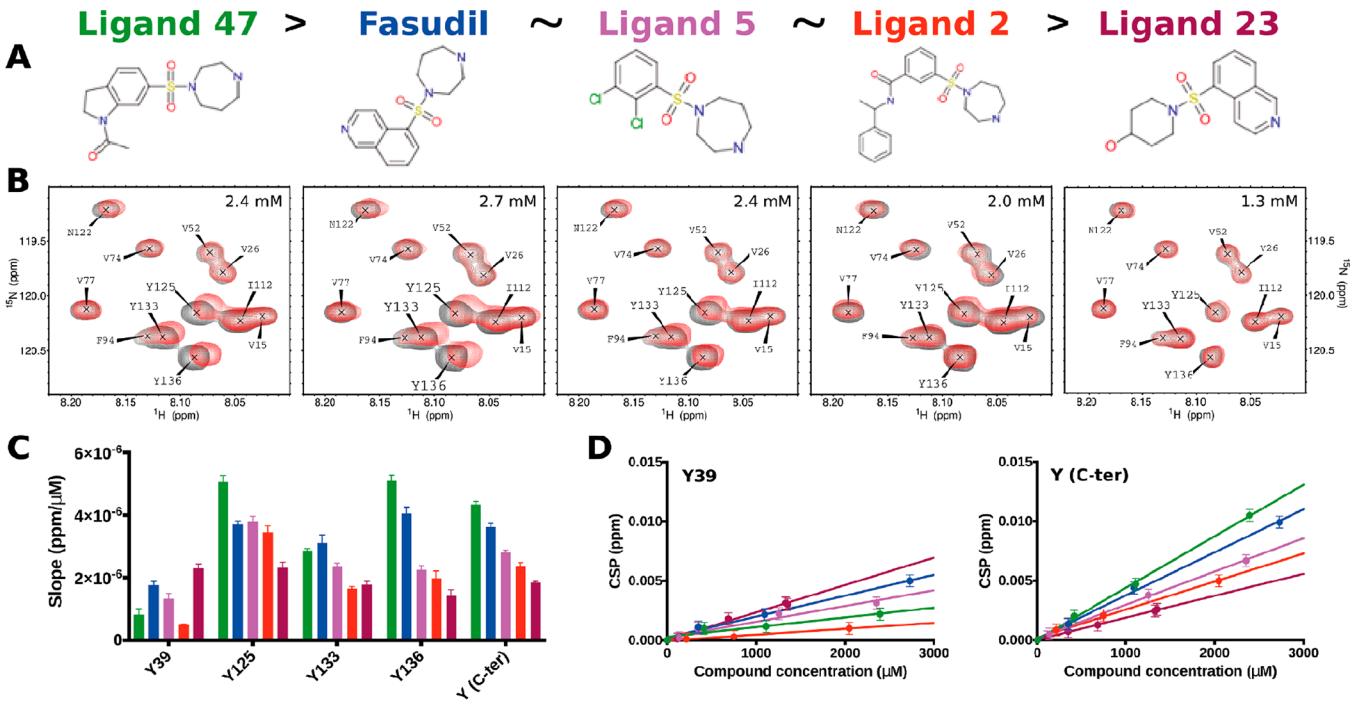

Figure 4. Predicted binding affinities of fasudil analogues with α-synuclein from simulation are in line with subsequently measured chemical shift perturbation titrations from NMR. (A) Structures of fasudil and tested analogues, with ligand 47 having the highest affinity for α-synuclein and ligand 23 the lowest. (B) NMR chemical shift titration curves of the aromatic residues of the C-terminal region of α-synuclein with the five ligands depicted in panel A. (C) Slope of titration curves for each tyrosine residue in α-synuclein, and the average of all tyrosine residues in the C-terminal region of α-synuclein (Y125, Y133, Y136). (D) Titration curves of each compound for Y39, and for the average of all tyrosine residues in the C-terminal region of α-synuclein. Individual titration curves for Y125, Y133, and Y136 are shown in Figure S10. The CSP errors are based on the resolution of the spectra.

shuttles back and forth among favorable interactions, remaining localized to the same region of α-syn.

Having obtained a better understanding of the binding interactions between fasudil and α-syn, we proceeded to test our model prospectively by simulating the binding of additional small molecules and then subsequently measuring the CSPs of a subset of the compounds by NMR. We selected 49 commercially available compounds containing variations of the isoquinoline, sulfonyl, and azepane scaffold of fasudil (Figure S9). We expected that these variations would influence available binding modes and affinity to α-syn. We then conducted a computational screen, in which we performed 60-μs simulations of each molecule with the α-syn-C-term fragment, and calculated the simulated dissociation constant, K_D, of each molecule (Table S3, Figure S9). The small molecule with the lowest K_D value (ligand 47), two molecules with K_D values similar to fasudil (ligands 2 and 5), and the ligand with the highest K_D value (ligand 23) are shown in Figure 4A along with fasudil.

The simulation results for the screened compounds could in some cases be explained based on their structure and information we learned from our fasudil simulations. Charge−charge interactions between fasudil and α-syn were important binding interactions observed in our simulations, for example, and in our screening simulations, molecules that did not have a positive charge (such as ligands 23 and 30) had higher K_D values, binding to α-syn-C-term ~2-fold more weakly compared to fasudil.

The simulation results of the strongest binder, ligand 47, would have been more difficult to deduce from the structure of the compound alone. Ligand 47 differs from fasudil by a change in the substitution position of the sulfonyl group relative to the ring system, and the addition of an acetyl group to a slightly modified ring system, and it was not immediately clear how these features may have resulted in its ~2-fold higher affinity to α-syn-C-term. To obtain improved statistics for these interactions, the simulation of α-syn-C-term and ligand 47 was extended to 200 μs. Examination of the interaction profile of ligand 47 with α-syn-C-term (Figure 3A) shows that the largest differences in the bound ensembles were an increased propensity for π-stacking in Y136 (in 7.5% of bound conformations compared to 4.8% of bound conformations for ligand 47 and fasudil, respectively) and the formation of hydrogen bonds between ligand 47 and P128, Y136, and P138 (in 1%, 2.5%, and 1.9% of bound conformations, respectively) that were not appreciably populated in the bound fasudil ensemble (0.2%, 1.0%, and 0.4% of bound conformations, respectively).

We also observed that the position of the sulfonyl group of ligand 47 relative to the ring system, and the corresponding change in the orientation of the charged amine of the azepane ring, seemed to increase the probability of forming multiple intermolecular interactions with α-syn-C-term simultaneously. The average mutual information between different protein−ligand interactions was slightly increased relative to fasudil (Figure S7), and we observed greater correlations between interaction pairs involving non-neighboring residues. In particular, we observed much stronger couplings among interaction pairs involving D135. In Figure 3B, we compare the conditional probabilities of observing additional intermolecular interactions for all conformations in which ligand 47 forms a charge contact with D135 to the corresponding

https://doi.org/10.1021/jacs.1c07591
J. Am. Chem. Soc. 2022, 144, 2501−2510

probabilities for fasudil. We observed that ligand 47 had increased conditional probabilities of forming π-stacking interactions with Y136 (13.4% vs 2.9%), hydrogen bond interactions with Y136 (11.5% vs 3.2%), hydrophobic contacts with Y136 (45.9% vs 31.8%).

Examination of configurations in which ligand 47 formed a charge interaction with D135 provides a possible explanation for these increases. The altered substitution position of the sulfonyl group oriented ligand 47 such that when it formed a charge interaction with D135, there was a dramatic increase in the asymmetry of π-stacking orientations with Y136: with the D135 charge interaction formed, orientations with $\beta < 90°$ were ~2.4-fold more populated than orientations with $\beta > 90°$ (Table S1, Figure S8). This stacking orientation also oriented the sulfonyl oxygens such that they were able to form hydrogen bonds with the amide of Y136, and positioned the additional acetyl group such that it was able to form hydrophobic contacts with Y136. A representative bound conformation of ligand 47 in its preferred stacking orientation and forming all 4 of these interactions is shown in Figure 3C.

We note that bound conformations in which ligand 47 simultaneously formed a hydrogen bond with Y136, aromatic stacking interactions with Y136, and charge contacts with D135 constitute <0.7% of the bound ensemble; conformations in which ligand 47 simultaneously formed a hydrogen bond with Y136 and aromatic stacking interactions with Y136 constitute <1.0% of the bound ensemble; conformations in which ligand 47 simultaneously formed a charge−charge contact with D135 and a hydrogen bond with Y136 constitute <1.3% of the bound ensemble; and conformations in which ligand 47 simultaneously formed a charge−charge contact with D135 and an aromatic stacking interaction with Y136 constitute <1.5% of the bound ensemble. This suggests that conformations that can simultaneously form all of these interactions, or pairs of these interactions, do not, by themselves, explain the increased affinity of ligand 47 for α-syn relative to fasudil, as the small population of these states cannot account for the ~2-fold increase in affinity. Instead, the increased affinity is better explained in the context of the dynamic shuttling model, in which these interactions are part of a larger network of transient and weak interactions that localize ligand 47 to these residues.

We next experimentally tested our computational predictions of relative binding affinities for a subset of screened compounds by measuring NMR CSPs of all α-syn residues in titrations of four ligands: ligand 47, ligand 23, ligand 5, and ligand 2 (Figure 4A). Due to solubility limitations of these molecules, it was not possible to saturate the observed CSPs and estimate K_D values directly. We instead estimated the relative affinities of the molecules by considering the slope of the CSPs measured for Y125, Y133, and Y136 during each titration, with larger slopes indicating higher affinities. We found that by taking the average slope observed for these tyrosine residues as a proxy for affinity to the C-terminal region of α-syn, the relative affinities of the five ligands estimated from the ligand titrations are in line with the affinities predicted from our MD simulations.

Interestingly, we observe that ligand 47 causes larger CSPs in Y136 and Y125 than does fasudil (Figures 4B and S10). This is consistent with the interaction profiles observed from our MD simulations, in which ligand 47 had a higher propensity to form hydrogen bonds and π-stacking interactions with Y136. The increased contact probability and stacking between ligand 47 and Y125 are also consistent with ligand 47's higher affinity than fasudil for Y125 observed by NMR. To examine whether ligand 47, like fasudil, had an increased propensity to interact with the C-terminal region of α-syn, we performed a 1.5 ms unbiased MD simulation of ligand 47 with full-length α-syn. We observed in this simulation that ligand 47, similarly to fasudil, had increased affinity for the C-terminal region of α-syn rather than exhibiting nonspecific affinity for all residues, in agreement with observed NMR CSPs (r = 0.68, Figure S11, Table S2).

Lastly, the experimentally tested ligands showed varying levels of affinity for Y39 in the NMR CSP titration experiments, and differed from the relative affinities observed at the C-terminus (Figure 4). Y39 has been shown to be key residue for modulation of α-syn aggregation by small molecules[57,58] as well as for α-syn dimerization in the oxidative environments persistent in disease states.[59] Of the experimentally tested ligands, ligand 23 showed the weakest affinity for the C-terminal region, something we also observed in the simulations, but had the strongest affinity for Y39 (Figure 4C). This prompted us to simulate the small molecules in our library with a fragment of α-syn from residues 29−49, in order to determine if our simulations would accurately capture the relative affinities between the tested compounds and Y39. We found that the simulations correctly identified ligand 23 as the strongest binder to the α-syn 29−49 fragment among the experimentally tested ligands, but did not capture well the overall relative affinities of ligands at Y39 (Figure 4, Table S3).

We also examined the binding of ligand 23 with full-length α-syn. Although the affinity of ligand 23 to Y39 in full-length α-syn is not the strongest relative to fasudil and ligand 47, we did find that, in contrast to fasudil and ligand 47, which heavily favored binding at the C-terminus relative to Y39, ligand 23 had a slight preference for Y39 (Table S2), in agreement with experiment. These results suggest that our MD simulations may be capable of differentiating between the affinities of small molecules to tyrosine residues in different sequence contexts.

CONCLUSION

We performed long-time-scale MD simulations of fasudil binding to α-syn and found, in agreement with NMR chemical shift perturbations, that fasudil prefers to bind to the C-terminal region of α-syn—a preference driven mainly by a combination of aromatic stacking and charge−charge interactions. The simulations provide an atomically detailed picture of the protein−ligand binding ensemble, illustrating how a network of weak and transient intermolecular interactions can lead to specific binding of a small molecule to a protein that remains highly dynamic.

The simulated binding mechanism observed here, in which the formation of specific intermolecular interactions orients ligands such that additional interactions are likely to form subsequently, provides a mechanistic explanation for how ligands can achieve sequence-specific binding with IDPs: fasudil bound, for example, with different affinities to the tyrosine-glutamate (YE) residue pairs at ^{125}YE^{126} and ^{136}YE^{137}, which appear in different sequence contexts. Based on the simulated binding mechanism, we can speculate that the pattern of charged and aromatic residues in IDPs is likely essential for dictating ligand binding specificity and affinity (e.g., a scrambled α-syn sequence with separated blocks of charged and aromatic residues would have large differences in

https://doi.org/10.1021/jacs.1c07591
J. Am. Chem. Soc. 2022, 144, 2501−2510

affinity and specificity compared to one with interspersed charged and aromatic residues).

We note that the dynamic shuttling mechanism described here provides a local description of IDP-ligand binding to a given binding site. Dynamic binding mechanisms such as those characterized in this study could potentially underlie IDP-ligand binding events in which the presence of a small molecule either reduces the conformational space accessible to an IDP in its bound state (sometimes referred to as "conformational restriction",[51] "population-shifting",[60] or "entropic collapse") or increases the conformational space accessible to an IDP in its bound state (sometimes referred to as "entropic expansion" [11,50]), and are not inherently associated with either thermodynamic binding scenario. The dynamic shuttling of a small molecule among heterogeneous binding modes could either stabilize a subset of conformations observed in the apo state of an IDP or increase the sampling of additional conformations not substantially populated in the apo state.

Although the simulations performed in this work focused on monomeric α-syn, and not on how monomers associate into oligomers and fibrils, we can speculate based on the simulated binding mechanism that fasudil may inhibit α-syn aggregation by hindering intermolecular protein−protein interactions preceding dimerization. In particular, studies[25,61−65] have shown that the C-terminal region may play an important role in the association of α-syn monomers, especially Y136 at the C terminus, a residue where we also see preferential binding of fasudil in our simulations. The binding of fasudil in the C-terminal region may screen protein−protein electrostatic attractions or sterically prevent the dimerization of two monomers.

In addition to confirming that simulations of fasudil and α-syn agreed retrospectively with previous NMR experiments, we prospectively tested the accuracy of our MD models by simulating α-syn with a library of 49 small molecules and testing the MD predictions with NMR measurements of a subset of these molecules. The experimentally determined relative binding affinities of these molecules were in line with our computational predictions, and the measured CSPs provided support for key structural features of the simulated binding interactions. These observations suggest potential strategies for the rational design of molecules that bind disordered protein sequences with higher affinity and greater specificity using insights from MD simulations.

■ ASSOCIATED CONTENT

Supporting Information

The Supporting Information is available free of charge at https://pubs.acs.org/doi/10.1021/jacs.1c07591.

Simulation methods; error estimation from blocking analyses; assessment of simulation convergence and accuracy; agreement of simulations of α-synuclein with previously reported NMR data from apo-α-synuclein; experimental methods; Tables S1−S7; and Figures S1−S20 (PDF)

■ AUTHOR INFORMATION

Corresponding Authors

Albert C. Pan − *D. E. Shaw Research, New York, New York 10036, United States*; Email: Albert.Pan@deshawresearch.com

Markus Zweckstetter − *German Center for Neurodegenerative Diseases (DZNE), 37077 Göttingen, Germany; Max Planck Institute for Biophysical Chemistry, 37077 Göttingen, Germany; DFG Research Center for Nanoscale Microscopy and Molecular Physiology of the Brain (CNMPB), 37073 Göttingen, Germany*; orcid.org/0000-0002-2536-6581; Email: markus.zweckstetter@dzne.de

David E. Shaw − *D. E. Shaw Research, New York, New York 10036, United States; Department of Biochemistry and Molecular Biophysics, Columbia University, New York, New York 10032, United States*; orcid.org/0000-0001-8265-5761; Email: David.Shaw@DEShawResearch.com

Authors

Paul Robustelli − *D. E. Shaw Research, New York, New York 10036, United States; Department of Chemistry, Dartmouth College, Hanover, New Hampshire 03755, United States*

Alain Ibanez-de-Opakua − *German Center for Neurodegenerative Diseases (DZNE), 37077 Göttingen, Germany*

Cecily Campbell-Bezat − *D. E. Shaw Research, New York, New York 10036, United States*

Fabrizio Giordanetto − *D. E. Shaw Research, New York, New York 10036, United States*; orcid.org/0000-0001-9876-9552

Stefan Becker − *Max Planck Institute for Biophysical Chemistry, 37077 Göttingen, Germany*

Complete contact information is available at: https://pubs.acs.org/10.1021/jacs.1c07591

Notes

The authors declare the following competing financial interest(s): This study was conducted and funded internally by D. E. Shaw Research, of which D.E.S. is the sole beneficial owner and Chief Scientist, and with which P.R., C.C.B., F.G., and A.C.P. are affiliated.

The MD trajectories of the simulations listed in Table S4 are available for noncommercial use through contacting trajectories@deshawresearch.com.

■ ACKNOWLEDGMENTS

The authors thank Michael Eastwood and Stefano Piana for helpful discussions, Berkman Frank for editorial assistance, and Karin Giller and Melanie Wegstroth for excellent help with NMR sample preparation. M.Z. was supported by the advanced grant "787679 -LLPS-NMR" of the European Research Council. Since June 2021, P.R.'s work at Dartmouth has been supported by the National Institutes of Health under award R35GM142750.

■ REFERENCES

(1) Van der Lee, R.; Buljan, M.; Lang, B.; Weatheritt, R. J.; Daughdrill, G. W.; Dunker, A. K.; Fuxreiter, M.; Gough, J.; Gsponer, J.; Jones, D. T.; Kim, P. M.; Kriwacki, R. W.; Oldfield, C. J.; Pappu, R. V.; Tompa, P.; Uversky, V. N.; Wright, P. E.; Babu, M. M. Classification of intrinsically disordered regions and proteins. *Chem. Rev.* **2014**, *114* (13), 6589−6631.

(2) Habchi, J.; Tompa, P.; Longhi, S.; Uversky, V. N. Introducing protein intrinsic disorder. *Chem. Rev.* **2014**, *114* (13), 6561−6588.

(3) Tompa, P. Intrinsically unstructured proteins. *Trends Biochem. Sci.* **2002**, *27* (10), 527−533.

(4) Dunker, A. K.; Cortese, M. S.; Romero, P.; Iakoucheva, L. M.; Uversky, V. N. Flexible nets. The roles of intrinsic disorder in protein interaction networks. *FEBS J.* **2005**, *272* (20), 5129−5148.

(5) Dyson, H. J.; Wright, P. E. Intrinsically unstructured proteins and their functions. *Nat. Rev. Mol. Cell Biol.* **2005**, *6* (3), 197−208.
(6) Wright, P. E.; Dyson, H. J. Intrinsically disordered proteins in cellular signaling and regulation. *Nat. Rev. Mol. Cell Biol.* **2015**, *16* (1), 18−29.
(7) Sormanni, P.; Piovesan, D.; Heller, G. T.; Bonomi, M.; Kukic, P.; Camilloni, C.; Fuxreiter, M.; Dosztanyi, Z.; Pappu, R. V.; Babu, M. M.; Longhi, S.; Tompa, P.; Dunker, A. K.; Uversky, V. N.; Tosatto, S. C.; Vendruscolo, M. Simultaneous quantification of protein order and disorder. *Nat. Chem. Biol.* **2017**, *13* (4), 339−342.
(8) Banani, S. F.; Lee, H. O.; Hyman, A. A.; Rosen, M. K. Biomolecular condensates: organizers of cellular biochemistry. *Nat. Rev. Mol. Cell Biol.* **2017**, *18* (5), 285−298.
(9) Babu, M. M.; van der Lee, R.; de Groot, N. S.; Gsponer, J. Intrinsically disordered proteins: regulation and disease. *Curr. Opin Struct Biol.* **2011**, *21* (3), 432−440.
(10) Heller, G. T.; Sormanni, P.; Vendruscolo, M. Targeting disordered proteins with small molecules using entropy. *Trends Biochem. Sci.* **2015**, *40* (9), 491−496.
(11) Heller, G. T.; Bonomi, M.; Vendruscolo, M. Structural ensemble modulation upon small-molecule binding to disordered proteins. *J. Mol. Biol.* **2018**, *430* (16), 2288−2292.
(12) Chen, J.; Liu, X.; Chen, J. Targeting intrinsically disordered proteins through dynamic interactions. *Biomolecules.* **2020**, *10* (5), 743.
(13) Fuertes, G; Nevola, L; Esteban-Martín, S. Perspectives on drug discovery strategies based on IDPs. *Intrinsically Disordered Proteins*; Academic Press: London, 2019; pp 275−327.
(14) Sadar, M. D. Discovery of drugs that directly target the intrinsically disordered region of the androgen receptor. *Expert Opin. Drug Discovery* **2020**, *15* (5), 551−560.
(15) De Mol, E.; Fenwick, R. B.; Phang, C. T.; Buzón, V.; Szulc, E.; de la Fuente, A.; Escobedo, A.; García, J.; Bertoncini, C. W.; Estébanez-Perpiñá, E.; McEwan, I. J.; Riera, A.; Salvatella, X. EPI-001, A compound active against castration-resistant prostate cancer, targets transactivation unit 5 of the androgen receptor. *ACS Chem. Biol.* **2016**, *11* (9), 2499−2505.
(16) Ruan, H.; Sun, Q.; Zhang, W.; Liu, Y.; Lai, L. Targeting intrinsically disordered proteins at the edge of chaos. *Drug Discov. Today.* **2019**, *24* (1), 217−227.
(17) Metallo, S. J. Intrinsically disordered proteins are potential drug targets. *Curr. Opin. Chem. Biol.* **2010**, *14* (4), 481−488.
(18) Iconaru, L. I.; Ban, D.; Bharatham, K.; Ramanathan, A.; Zhang, W.; Shelat, A. A.; Zuo, J.; Kriwacki, R. W. Discovery of small molecules that inhibit the disordered protein, p27(Kip1). *Sci. Rep.* **2015**, *5*, 15686.
(19) Bonomi, M.; Heller, G. T.; Camilloni, C.; Vendruscolo, M. Principles of protein structural ensemble determination. *Curr. Opin. Struct. Biol.* **2017**, *42*, 106−116.
(20) Jensen, M. R.; Ruigrok, R. W.; Blackledge, M. Describing intrinsically disordered proteins at atomic resolution by NMR. *Curr. Opin. Struct. Biol.* **2013**, *23* (3), 426−435.
(21) Wu, K. P.; Baum, J. Detection of transient interchain interactions in the intrinsically disordered protein alpha-synuclein by NMR paramagnetic relaxation enhancement. *J. Am. Chem. Soc.* **2010**, *132* (16), 5546−5547.
(22) Sung, Y. H.; Eliezer, D. Residual structure, backbone dynamics, and interactions within the synuclein family. *J. Mol. Biol.* **2007**, *372* (3), 689−707.
(23) Jin, F.; Yu, C.; Lai, L.; Liu, Z. Ligand clouds around protein clouds: a scenario of ligand binding with intrinsically disordered proteins. *PLoS Comput. Biol.* **2013**, *9* (10), e1003249.
(24) Karpinar, D. P.; Balija, M. B.; Kügler, S.; Opazo, F.; Rezaei-Ghaleh, N.; Wender, N.; Kim, H. Y.; Taschenberger, G.; Falkenburger, B. H.; Heise, H.; Kumar, A.; Riedel, D.; Fichtner, L.; Voigt, A.; Braus, G. H.; Giller, K.; Becker, S.; Herzig, A.; Baldus, M.; Jäckle, H.; Eimer, S.; Schulz, J. B.; Griesinger, C.; Zweckstetter, M. Pre-fibrillar alpha-synuclein variants with impaired beta-structure increase neurotoxicity in Parkinson's disease models. *EMBO J.* **2009**, *28* (20), 3256−3268.
(25) Tatenhorst, L.; Eckermann, K.; Dambeck, V.; Fonseca-Ornelas, L.; Walle, H.; Lopes da Fonseca, T.; Koch, J. C.; Becker, S.; Tönges, L.; Bähr, M.; Outeiro, T. F.; Zweckstetter, M.; Lingor, P. Fasudil attenuates aggregation of α-synuclein in models of Parkinson's disease. *Acta Neuropathol Commun.* **2016**, *4*, 39.
(26) Granata, D.; Baftizadeh, F.; Habchi, J.; Galvagnion, C.; De Simone, A.; Camilloni, C.; Laio, A.; Vendruscolo, M. The inverted free energy landscape of an intrinsically disordered peptide by simulations and experiments. *Sci. Rep.* **2015**, *5*, 15449.
(27) Lindorff-Larsen, K.; Trbovic, N.; Maragakis, P.; Piana, S.; Shaw, D. E. Structure and dynamics of an unfolded protein examined by molecular dynamics simulation. *J. Am. Chem. Soc.* **2012**, *134* (8), 3787−3791.
(28) Tóth, G.; Gardai, S. J.; Zago, W.; Bertoncini, C. W.; Cremades, N.; Roy, S. L.; Tambe, M. A.; Rochet, J. C.; Galvagnion, C.; Skibinski, G.; Finkbeiner, S.; Bova, M.; Regnstrom, K.; Chiou, S. S.; Johnston, J.; Callaway, K.; Anderson, J. P.; Jobling, M. F.; Buell, A. K.; Yednock, T. A.; Knowles, T. P.; Vendruscolo, M.; Christodoulou, J.; Dobson, C. M.; Schenk, D.; McConlogue, L. Targeting the intrinsically disordered structural ensemble of α-synuclein by small molecules as a potential therapeutic strategy for Parkinson's disease. *PLoS One.* **2014**, *9* (2), e87133.
(29) Salvi, N.; Abyzov, A.; Blackledge, M. Solvent-dependent segmental dynamics in intrinsically disordered proteins. *Sci. Adv.* **2019**, *5* (6), eaax2348.
(30) Salvi, N.; Abyzov, A.; Blackledge, M. Analytical description of NMR relaxation highlights correlated dynamics in intrinsically disordered proteins. *Angew. Chem., Int. Ed. Engl.* **2017**, *56* (45), 14020−14024.
(31) Robustelli, P.; Trbovic, N.; Friesner, R. A.; Palmer, A. G., III Conformational dynamics of the partially disordered yeast transcription factor GCN4. *J. Chem. Theory Comput.* **2013**, *9* (11), 5190.
(32) Huang, J.; Rauscher, S.; Nawrocki, G.; Ran, T.; Feig, M.; de Groot, B. L.; Grubmüller, H.; MacKerell, A. D., Jr. CHARMM36m: an improved force field for folded and intrinsically disordered proteins. *Nat. Methods* **2017**, *14* (1), 71−73.
(33) Robustelli, P.; Piana, S.; Shaw, D. E. Developing a molecular dynamics force field for both folded and disordered protein states. *Proc. Natl. Acad. Sci. U. S. A.* **2018**, *115* (21), E4758−E4766.
(34) Nerenberg, P. S.; Jo, B.; So, C.; Tripathy, A.; Head-Gordon, T. Optimizing solute-water van der Waals interactions to reproduce solvation free energies. *J. Phys. Chem. B* **2012**, *116* (15), 4524−4534.
(35) Best, R. B.; Zheng, W.; Mittal, J. Balanced protein-water interactions improve properties of disordered proteins and non-specific protein association. *J. Chem. Theory Comput.* **2014**, *10* (11), 5113−5124.
(36) Piana, S.; Donchev, A. G.; Robustelli, P.; Shaw, D. E. Water dispersion interactions strongly influence simulated structural properties of disordered protein states. *J. Phys. Chem. B* **2015**, *119* (16), 5113−5123.
(37) Piana, S.; Robustelli, P.; Tan, D.; Chen, S.; Shaw, D. E. Development of a force field for the simulation of single-chain proteins and protein-protein complexes. *J. Chem. Theory Comput.* **2020**, *16* (4), 2494−2507.
(38) Tian, C.; Kasavajhala, K.; Belfon, K. A. A.; Raguette, L.; Huang, H.; Migues, A. N.; Bickel, J.; Wang, Y.; Pincay, J.; Wu, Q.; Simmerling, C. ff19SB: Amino-acid-specific protein backbone parameters trained against quantum mechanics energy surfaces in solution. *J. Chem. Theory Comput.* **2020**, *16* (1), 528−552.
(39) Shabane, P. S.; Izadi, S.; Onufriev, A. V. General purpose water model can improve atomistic simulations of intrinsically disordered proteins. *J. Chem. Theory Comput.* **2019**, *15* (4), 2620−2634.
(40) Song, D.; Luo, R.; Chen, H. F. The IDP-specific force field ff14IDPSFF improves the conformer sampling of intrinsically disordered proteins. *J. Chem. Inf Model.* **2017**, *57* (5), 1166−1178.
(41) Yu, L.; Li, D. W.; Brüschweiler, R. Balanced amino-acid-specific molecular dynamics force field for the realistic simulation of both

https://doi.org/10.1021/jacs.1c07591
J. Am. Chem. Soc. 2022, 144, 2501−2510

folded and disordered proteins. *J. Chem. Theory Comput.* **2020**, *16* (2), 1311−1318.
(42) Robustelli, P.; Piana, S.; Shaw, D. E. Mechanism of coupled folding-upon-binding of an intrinsically disordered protein. *J. Am. Chem. Soc.* **2020**, *142* (25), 11092−11101.
(43) Conicella, A. E.; Dignon, G. L.; Zerze, G. H.; Schmidt, H. B.; D'Ordine, A. M.; Kim, Y. C.; Rohatgi, R.; Ayala, Y. M.; Mittal, J.; Fawzi, N. L. TDP-43 α-helical structure tunes liquid-liquid phase separation and function. *Proc. Natl. Acad. Sci. U. S. A.* **2020**, *117* (11), 5883−5894.
(44) Paloni, M.; Bailly, R.; Ciandrini, L.; Barducci, A. Unraveling molecular interactions in liquid-liquid phase separation of disordered proteins by atomistic simulations. *J. Phys. Chem. B* **2020**, *124* (41), 9009−9016.
(45) Zheng, W.; Dignon, G. L.; Jovic, N.; Xu, X.; Regy, R. M.; Fawzi, N. L.; Kim, Y. C.; Best, R. B.; Mittal, J. Molecular details of protein condensates probed by microsecond long atomistic simulations. *J. Phys. Chem. B* **2020**, *124* (51), 11671−11679.
(46) Convertino, M.; Vitalis, A.; Caflisch, A. Disordered binding of small molecules to Aβ(12−28). *J. Biol. Chem.* **2011**, *286* (48), 41578−41588.
(47) Li, G.; Pomès, R. Binding mechanism of inositol stereoisomers to monomers and aggregates of Aβ(16−22). *J. Phys. Chem. B* **2013**, *117* (22), 6603−6613.
(48) Tarus, B.; Nguyen, P. H.; Berthoumieu, O.; Faller, P.; Doig, A. J.; Derreumaux, P. Molecular structure of the NQTrp inhibitor with the Alzheimer Aβ1−28 monomer. *Eur. J. Med. Chem.* **2015**, *91*, 43−50.
(49) Heller, G. T.; Aprile, F. A.; Michaels, T. C. T.; Limbocker, R.; Perni, M.; Ruggeri, F. S.; Mannini, B.; Löhr, T.; Bonomi, M.; Camilloni, C.; De Simone, A.; Felli, I. C.; Pierattelli, R.; Knowles, T. P. J.; Dobson, C. M.; Vendruscolo, M. Small-molecule sequestration of amyloid-β as a drug discovery strategy for Alzheimer's disease. *Sci. Adv.* **2020**, *6* (45), eabb5924.
(50) Heller, G. T.; Aprile, F. A.; Bonomi, M.; Camilloni, C.; De Simone, A.; Vendruscolo, M. Sequence specificity in the entropy-driven binding of a small molecule and a disordered peptide. *J. Mol. Biol.* **2017**, *429* (18), 2772−2779.
(51) Herrera-Nieto, P.; Pérez, A.; De Fabritiis, G. Small molecule modulation of intrinsically disordered proteins using molecular dynamics simulations. *J. Chem. Inf Model.* **2020**, *60* (10), 5003−5010.
(52) Liang, C.; Savinov, S. N.; Fejzo, J.; Eyles, S. J.; Chen, J. Modulation of Amyloid-β42 Conformation by small molecules through nonspecific binding. *J. Chem. Theory Comput.* **2019**, *15* (10), 5169−5174.
(53) Michel, J.; Cuchillo, R. The impact of small molecule binding on the energy landscape of the intrinsically disordered protein C-myc. *PLoS One.* **2012**, *7* (7), e41070.
(54) Wang, J.; Wang, W.; Kollman, P. A.; Case, D. A. Automatic atom type and bond type perception in molecular mechanical calculations. *J. Mol. Graph Model.* **2006**, *25* (2), 247−260.
(55) Wang, J.; Wolf, R. M.; Caldwell, J. W.; Kollman, P. A.; Case, D. A. Development and testing of a general amber force field. *J. Comput. Chem.* **2004**, *25* (9), 1157−1174.
(56) Chelli, R.; Gervasio, F. L.; Procacci, P.; Schettino, V. Stacking and T-shape competition in aromatic-aromatic amino acid interactions. *J. Am. Chem. Soc.* **2002**, *124* (21), 6133−6143.
(57) Lamberto, G. R.; Binolfi, A.; Orcellet, M. L.; Bertoncini, C. W.; Zweckstetter, M.; Griesinger, C.; Fernández, C. O. Structural and mechanistic basis behind the inhibitory interaction of PcTS on alpha-synuclein amyloid fibril formation. *Proc. Natl. Acad. Sci. U. S. A.* **2009**, *106* (50), 21057−21062.
(58) Fonseca-Ornelas, L.; Eisbach, S. E.; Paulat, M.; Giller, K.; Fernández, C. O.; Outeiro, T. F.; Becker, S.; Zweckstetter, M. Small molecule-mediated stabilization of vesicle-associated helical α-synuclein inhibits pathogenic misfolding and aggregation. *Nat. Commun.* **2014**, *5*, 5857.
(59) Al-Hilaly, Y. K.; Biasetti, L.; Blakeman, B. J.; Pollack, S. J.; Zibaee, S.; Abdul-Sada, A.; Thorpe, J. R.; Xue, W. F.; Serpell, L. C. The involvement of dityrosine crosslinking in α-synuclein assembly and deposition in Lewy Bodies in Parkinson's disease. *Sci. Rep.* **2016**, *6*, 39171.
(60) Ban, D.; Iconaru, L. I.; Ramanathan, A.; Zuo, J.; Kriwacki, R. W. A small molecule causes a population shift in the conformational landscape of an intrinsically disordered protein. *J. Am. Chem. Soc.* **2017**, *139* (39), 13692−13700.
(61) Li, W.; West, N.; Colla, E.; Pletnikova, O.; Troncoso, J. C.; Marsh, L.; Dawson, T. M.; Jakala, P.; Hartmann, T.; Price, D. L.; Lee, M. K. Aggregation promoting C-terminal truncation of -synuclein is a normal cellular process and is enhanced by the familial Parkinson's disease-linked mutations. *Proceedings of the National Academy of Sciences.* **2005**, *102*, 2162−2167.
(62) Liu, C.-W.; Giasson, B. I.; Lewis, K. A.; Lee, V. M.; DeMartino, G. N.; Thomas, P. J. A Precipitating Role for Truncated α-Synuclein and the Proteasome in α-Synuclein Aggregation. *J. Biol. Chem.* **2005**, *280*, 22670−22678.
(63) Hoyer, W.; Cherny, D.; Subramaniam, V.; Jovin, T. M. Impact of the Acidic C-Terminal Region Comprising Amino Acids 109−140 on α-Synuclein Aggregation in Vitro. *Biochemistry* **2004**, *43*, 16233−16242.
(64) Izawa, Y.; Tateno, H.; Kameda, H.; Hirakawa, K.; Hato, K.; Yagi, H.; Hongo, K.; Mizobata, T.; Kawata, Y. Role of C -terminal negative charges and tyrosine residues in fibril formation of α-synuclein. *Brain Behav.* **2012**, *2*, 595−605.
(65) Levitan, K.; Chereau, D.; Cohen, S. I. A.; Knowles, T. P. J.; Dobson, C. M.; Fink, A. L.; Anderson, J. P.; Goldstein, J. M.; Millhauser, G. L. Conserved C-Terminal Charge Exerts a Profound Influence on the Aggregation Rate of α-Synuclein. *J. Mol. Biol.* **2011**, *411*, 329−333.

https://doi.org/10.1021/jacs.1c07591
J. Am. Chem. Soc. 2022, 144, 2501−2510